

# How Low Can You Go? Surfacing Prototypical In-Distribution Samples for Unsupervised Anomaly Detection

Felix Meissen<sup>1</sup>, Johannes Getzner<sup>1</sup>, Alexander Ziller<sup>1</sup>, Georgios Kaissis<sup>1,2</sup>, Daniel Rückert<sup>1,3</sup>

<sup>1</sup>Technical University of Munich <sup>2</sup>Helmholtz Zentrum Munich <sup>3</sup>Imperial College London

felix.meissen@tum.de

## Abstract

*Unsupervised anomaly detection (UAD) alleviates large labeling efforts by training exclusively on unlabeled in-distribution data and detecting outliers as anomalies. Generally, the assumption prevails that large training datasets allow the training of higher-performing UAD models. However, in this work, we show that using only very few training samples can already match – and in some cases even improve – anomaly detection compared to training with the whole training dataset. We propose three methods to identify prototypical samples from a large dataset of in-distribution samples. We demonstrate that by training with a subset of just ten such samples, we achieve an area under the receiver operating characteristics curve (AUROC) of 96.37% on CIFAR10, 92.59% on CIFAR100, 95.37% on MNIST, 95.38% on Fashion-MNIST, 96.37% on MVTEC-AD, 98.81% on BraTS, and 81.95% on RSNA pneumonia detection, even exceeding the performance of full training in 25/67 classes we tested. Additionally, we show that the prototypical in-distribution samples identified by our proposed methods translate well to different models and other datasets and that using their characteristics as guidance allows for successful manual selection of small subsets of high-performing samples. Our code is available at [https://anonymous.4open.science/r/uad\\_prototypical\\_samples/](https://anonymous.4open.science/r/uad_prototypical_samples/)*

## 1. Introduction

Unsupervised anomaly detection (UAD) or out-of-distribution (OOD) detection aims to distinguish samples from an in-distribution (ID) from any sample that stems from another distribution. Machine learning models are typically used for this task. The machine learning model learns to represent the in-distribution by using only samples from that distribution for training. The trained model detects OOD samples via their distance to the in-distribution. UAD has several vital applications in computer vision: It

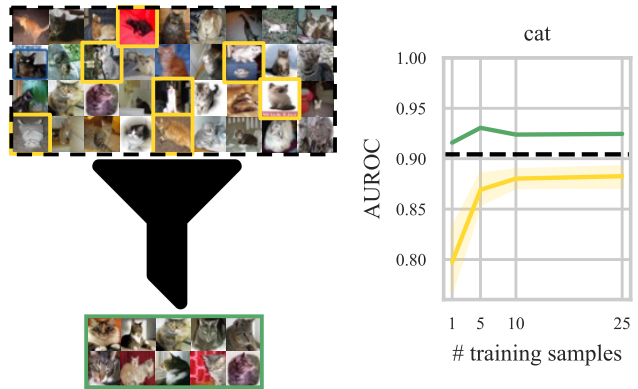


Figure 1. Selecting only a few prototypical in-distribution samples (revealed by our method) for training can achieve higher anomaly detection performance than training with 100% of the available data. Results for anomaly detection on the *cat* class from CIFAR10. Black dashed: whole training set. Yellow: randomly selected samples including standard deviations over different random selections. Green: Best-performing samples identified with our method.

is used to detect pathological samples in medical images [6, 23, 28, 35], to spot defects in industrial manufacturing [3, 10, 14, 33], or as safeguards to filter unsuitable input data for supervised downstream models, for example, in autonomous driving.

In deep learning, the prevailing assumption is that more data leads to better models. However, large amounts of – especially labeled – data are often difficult and costly to obtain and not always available. There exist numerous indications that for UAD models only a fraction of the resources commonly used are necessary: Many anomaly detection models converge very fast during training, small models achieve similar performance compared to larger ones, and training with only a few samples can already give reasonable performance. Despite these early evidences, only a handful of works have included analyses of training UAD models with few resources. Roth et al. [33] and Lagogiannis et al. [23] had single experiments with small sample sizes in their

work, but so far, none have investigated the phenomenon in detail. Training with only very few samples would, however, have numerous advantages: Small datasets are cheap and easy to obtain and also available for a wide variety of tasks. Further, training on such datasets is incredibly time- and resource-efficient, enabling widespread deployment while mitigating the environmental impact by reducing the CO<sub>2</sub> emissions associated with the energy consumption of such machine learning models.

In this paper, we present findings showing that only very few training samples are necessary to achieve similar or even better anomaly detection performance compared to training with 100% of the available training data (which we denote as “full training” in the remainder of the manuscript). Specifically, we propose three methods for selecting a high-performing subset of samples from the initial training dataset, as depicted in Fig. 1. The samples detected by our proposed methods are prototypical in-distribution samples for each dataset and shine light upon the question of what “normality” constitutes for anomaly detection models. Our findings, therefore, allow for more performant, robust, and interpretable anomaly detection. In addition to compelling experimental results on multiple dataset, models, and domains, we provide theoretical justification why the training subsets identified by our methods achieve good anomaly detection performance. In summary, the main contributions of this paper are:

- We show that only very few training samples can suffice for state-of-the-art performance in UAD.
- We propose three methods to automatically find prototypical in-distribution samples for a given class and describe their common characteristics.
- We further demonstrate how the methods used in our study can effectively filter out noisy or corrupted data points from the initial training dataset.
- Lastly, we show that the prototypical samples surfaced by our method and their characteristics translate to equally good performance for other models, datasets, and even tasks.

## 2. Related work

Our work contains components from both anomaly detection and core-set selection. Here, we give a brief overview of these concepts and related research work.

### 2.1. Anomaly detection

Anomaly detection is deeply rooted in computer vision, with many influential works benchmarking their models on natural-image datasets, such as CIFAR10, CIFAR100 [22], MNIST [24], or Fashion-MNIST [39]. Early works were mostly based on (Variational) Autoencoders [1, 21, 26, 43] or Generative Adversarial Networks [2, 12, 31] trying to restrict the learned manifold of the generative model. The

model will then faithfully reconstruct in-distribution samples, whereas OOD samples can be detected due to their large reconstruction errors. Also, one-class classification models [34] or such that learn surrogate tasks [7, 17] have been successfully used. More recently, works that use pre-trained neural networks (such as ResNets [19]) have become popular and still are the best-performing models for these datasets [8], of which we also utilize the model by Reiss et al. [32] in our experiments.

The release of MVTec-AD [10] for industrial defect detection sparked a whole line of research around this dataset as it was the first to contain a variety of useful, real-world anomaly detection tasks. After early attempts to solve these with various techniques, including Autoencoders [9] and knowledge distillation methods [11], research converged on self-supervised approaches [25, 41], ResNets pre-trained on ImageNet [13, 14, 33], or combinations thereof [3]. In this study, we use PatchCore by Roth et al. [33] because of its simplicity and competitive performance on MVTec-AD.

Anomaly detection was also successfully applied in medical computer vision, where it is used to discriminate samples from healthy subjects (in-distribution) from diseased ones (outliers). Schlegl et al. [35] have successfully discovered biomarkers in retinal OCT images using a GAN. To detect tumors and lesions in brain MRI, numerous Autoencoder-based approaches [5, 40, 45] and Diffusion models [38] have been proposed. Furthermore, anomaly detection has been successfully applied in Chest X-ray images to detect COVID-19 [42] or other diseases [23, 27]. For the medical datasets in this work, we use FAE [28], as it was the best-performing model in the comparative study by Lagogiannis et al. [23].

### 2.2. Core-set selection

Core-set selection aims to create a small informative dataset such that the models trained on these samples show a similar test performance compared to those trained on the original dataset. Core-set selection techniques for deep learning include minimizing the feature-space distance [37] or the distance of gradients with respect to a neural network [30] between the selected subset and the original dataset. In anomaly detection, core-set selection has been used by Roth et al. [33]. Here, however, the selection is done on patch features instead of images. In MemAE, Gong et al. [18] restricted the latent space of an Autoencoder to a set of learned in-distribution feature vectors to perform anomaly detection. While this work also finds prototypical feature vectors, they again cannot be translated back to images and, consequently, cannot be used for core-set selection.

### 3. Surfacing prototypical in-distribution samples through core-set selection

Anomaly detection models are usually trained on large datasets. By evaluating the detection error that can be achieved by training with single samples, we aim to identify characteristics of samples that can be used to create small but high-performing training datasets. Mathematically, we want to determine a subset  $D_{\text{sub}}$  with  $M \in \mathbb{N}$  samples from the original dataset  $D$  with  $N \in \mathbb{N}$  samples denoted as  $x_i \in \mathbb{R}^D$  with  $i = 1, 2, \dots, N$ , such that:

$$\begin{aligned} &\text{minimize } E(D_{\text{sub}}, \psi, D_{\text{val}}) \quad \text{subject to} \\ &M < N, \\ &D_{\text{sub}} \subset D, \text{ and } |D_{\text{sub}}| = M, \end{aligned} \quad (1)$$

where  $E(D_{\text{sub}}, \psi, D_{\text{val}})$  is the detection error produced by a model  $\psi$  trained on  $D_{\text{sub}}$  and evaluated on the validation set  $D_{\text{val}} = \{(x_1, y_1), \dots, (x_K, y_K)\}$ ,  $x_k \in \mathbb{R}^D$ ,  $y_k \in \{-1, +1\}$ . Since OOD samples should receive higher anomaly scores than in-distribution samples, the labels  $-1$  and  $+1$  correspond to ID and OOD samples, respectively.

**Greedy selection** Since it is possible to train UAD models with only one sample, we can heuristically estimate the quality of each sample individually as  $E(\{x_i\}, \psi, D_{\text{val}})$  for  $i = 1, 2, \dots, N$ . From this information, we construct  $D_{\text{sub}}$  as:

$$D_{\text{sub}} = \arg \min_{\{x_j | x_j \in D, 1 \leq j \leq M\}} \sum_{j=1}^M E(\{x_j\}, \psi, D_{\text{val}}). \quad (2)$$

In our work, we select the AUROC as the optimization target  $E$ . Note that the set of samples that produce the smallest errors is not necessarily equal to the set of samples that together produce the lowest error, but is a good approximation thereof, as we will later see in Sec. 4.3.

**Evolutionary algorithm** While the greedy approach above is fast, easy to implement, and intuitive, it prefers subsets of visually similar samples, as we will later show. This is desirable in some cases, however, there are also scenarios where multiple of normal samples should be covered in the dataset. To get a better coverage of the normal variations in a dataset, we propose a second approach described in the following. For each combination of a training sample  $x_i \in D$  and a validation sample  $x_k \in D_{\text{val}}$ , we compute an anomaly score  $s(x_i, x_k)$  by training the anomaly detection model on  $x_i$  only and running inference on  $x_j$ . The objective is to find a subset  $D_{\text{sub}} = \{x_i | x_i \in D, 1 \leq i \leq M\}$  that maximizes a fitness function  $f$  described as:

$$f(D_{\text{sub}}) = \sum_{x_k, y_k \in D_{\text{val}}} \max_{x_j \in D_{\text{sub}}} y_k \cdot s(x_j, x_k). \quad (3)$$

Maximizing  $f$  allows for finding  $M$  training samples  $x_i$  that achieve best performance in classifying validation samples  $x_k$  as ID or OOD. Since this problem is  $\mathcal{NP}$ -hard, we approximate the solution using an evolutionary algorithm:

---

#### Algorithm 1: Evolutionary Algorithm

---

**Data:** Training dataset  $D$ , validation dataset  $D_{\text{val}}$ , population size  $P$ , anomaly scores  $s(x_i, x_k) \forall x_i \in D, x_k \in D_{\text{val}}$ , fitness function  $f$ , number of generations  $G$

**Result:** Approximately optimal subset  $D_{\text{sub}}^*$

Initialize a random population

$\mathcal{P} = \{D_{\text{sub},p} | 1 \leq p \leq P\}$ ;

**for**  $gen \leftarrow 1$  **to**  $G$  **do**

    Evaluate the fitness function  $f$  for each individual  $D_{\text{sub},p} \in \mathcal{P}$ ;

    Remove the least-fit  $\frac{P}{2}$  individuals  $D_{\text{sub},p} \in \mathcal{P}$  from  $\mathcal{P}$  to determine the best subset  $\mathcal{P}'$ ;

    Randomly apply either a crossover (combine two individuals) or mutation (replace one sample) operation to each individual in  $\mathcal{P}'$  to create a modified population  $\mathcal{P}''$ ;

    Generate a new population  $\mathcal{P} = \mathcal{P}' \cup \mathcal{P}''$ ;

**end**

**return** *Best individual found in the final population*;

---

In the crossover operation, random subsets of two individuals  $D_{\text{sub},1}, D_{\text{sub},2} \in \mathcal{P}'$  (called parents) are merged to produce a new individual  $D'_{\text{sub}}$ , such that  $|D'_{\text{sub}}| = M$ . In the mutation operation, one sample  $x_1 \in D_{\text{sub}}$  of an individual  $D_{\text{sub}} \in \mathcal{P}'$  is randomly replaced with another sample  $x_2 \in D \setminus D_{\text{sub}}$  to produce a new individual  $D'_{\text{sub}}$ :

$$D'_{\text{sub}} = D_{\text{sub}} \setminus \{x_1\} \cup \{x_2\}. \quad (4)$$

In contrast to the greedy selection strategy that favors visually similar samples, the subsets found by the evolutionary algorithm have better coverage of the different notions of normality contained in the training dataset (cf. Fig. 3). However, note that such a better coverage could also be harmful when the normal dataset is noisy, i.e., it contains samples that should be considered abnormal. These are more effectively filtered out using greedy selection.

**Core-set selection** As we will see in Sec. 4, both the greedy selection and the evolutionary algorithm identify well-performing, prototypical inlier samples. Both methods, however, require a labeled validation set. The selected

samples might therefore be bias towards this the distribution of this specific validation set. Since anomaly detection often deals with “unknown unknowns” – i.e. outlier types that are not known beforehand – it would be desirable to perform the selection only based on the in-distribution data. Hence, we add another sample-selection method for the PANDA model that requires only information from the in-distribution training data. Given the neural network  $\psi_0$  (cf. Suppl. material Sec. 8), we compute the  $d$ -dimensional latent codes of all samples in the training set:  $z_i = \psi_0(x_i) \forall x_i \in D, z_i \in \mathbb{R}^d$ . Next, we perform core-set selection using a Gaussian Mixture Model (GMM) with  $M$  components fitted to this latent space. Let  $\mathcal{G} = \{\mu_1, \mu_2, \dots, \mu_M\}$  represent the set of means (centroids) of the  $M$  components of the GMM, where  $\mu_j$  denotes the mean of the  $j$ -th component. As core-set samples, we choose the images corresponding to the latent codes that are closest to the centroids:

$$\arg \min_{x_i \in D} \|\psi_0(x_i) - \mu_j\|_2 \quad \forall \mu_j \in \mathcal{G}. \quad (5)$$

The intuition behind this strategy is that compared to randomly selecting samples, the core-set selection better covers different parts of the in-distribution. we only tested the core-set selection strategy for the PANDA model since the latent spaces of FAE and PatchCore are too high-dimensional to trivially fit a GMM in them.

## 4. Experiments and results

### 4.1. Datasets and models

To evaluate our methods, we use datasets from the natural- and medical-image domains, showing the applicability of our method in diverse tasks. CIFAR10, CIFAR100 [22], MNIST [24], and Fashion-MNIST [39] are trained in a one-vs-rest setting where one class is used as the in-distribution, and all other classes are combined as outliers. MVTec-AD [10] is an industrial defect detection dataset and a frequently used benchmark for UAD models. In the Chest X-ray images of the RSNA Pneumonia Detection dataset [36], the in-distribution constitutes images of healthy patients, while anomalous samples show signs of pneumonia or other lung opacities. In addition, we use CheXpert [20] to test if the samples found by our method generalize to other datasets. Similarly to RSNA, the in-distribution samples here are images labeled with “No Finding”, while OOD samples either display pneumonia or other lung opacities. Lastly, we detect MRI slices with glioma the BraTS dataset [4, 29]. For each dataset, we chose a respective state-of-the-art model: PANDA [32] is used for CIFAR10, CIFAR100, MNIST, and Fashion-MNIST, PatchCore [33] for MVTec-AD, and FAE [23, 28] for RSNA, CheXpert and BraTS. We additionally used Reverse Distillation (RD) by Deng and Li [14] for RSNA to test the generalizability of identified samples

across models. Details about the datasets and models are in the supplementary material.

### 4.2. Experimental setup

As suggested by Reiss et al. [32], we train PANDA for a constant number of 2355 steps (corresponding to 15 epochs on CIFAR10) using the SGD optimizer with a learning rate of 0.01 and weight decay of 0.00005. FAE converges very fast on BraTS, RSNA, and CheXpert, so it was trained for 500 steps using the Adam optimizer with a learning rate of 0.0002. In our experiments, the evolutionary algorithm was robust to the population size  $P$  and the number of generations  $G$ . In all experiments, we therefore empirically set  $P = 1000$  and  $G = 500$ . For all models, we used the official PyTorch implementations by the authors. Because of compute limitations, we only compute  $E(x_i, \psi, D_{\text{sub}})$  and  $s(x_j, x_k) \forall x_k \in D_{\text{val}}$  for a subset of  $D$  with size  $K = 300$  samples for every dataset except RSNA. We further restricted the maximum subset size to  $M = 25$  samples in our experiments as we did not experience substantial increases in performance beyond this point. Multiplied by the number of experiments and selection strategies, this decision saved significant amounts of our limited resources and allowed for more extensive experimentation in other dimensions.

### 4.3. A few selected samples can outperform training with the whole dataset

We find that UAD models achieve high performance even when trained with only a few samples. As depicted in Fig. 2, PANDA achieves close to full training performance on CIFAR10 when using only the top ten samples identified by our greedy selection method, already surpassing the full training performance in four out of ten classes (cf. suppl. material, Tab. 3). Notably, with more than five samples for the “bird” and “cat” classes, performance starts to degrade again. Tab. 1 shows that this phenomenon is not specific to CIFAR10 and PANDA but generalizes across all datasets and models used in this study. It also shows that our evolutionary strategy performs similarly well or even better on some datasets, outperforming full training on MVTec-AD, BraTS, and RSNA. Core-set selection with a GMM performs consistently better than random and outperforms the other two strategies on CIFAR100 and MNIST, despite not using any labels. Notably, even though our selection strategies generally perform better, random selection of samples already gives high performance. The gap between random and informed selection becomes more pronounced when using less and less samples. In 25/67 classes tested in this study, training with at most 25 samples outperforms training with the full dataset, and the best performance on RSNA in our experiments is achieved with as little as 0.3% of the full training data. These results show that there exist samples in many datasets whose inclusion degrades performance.

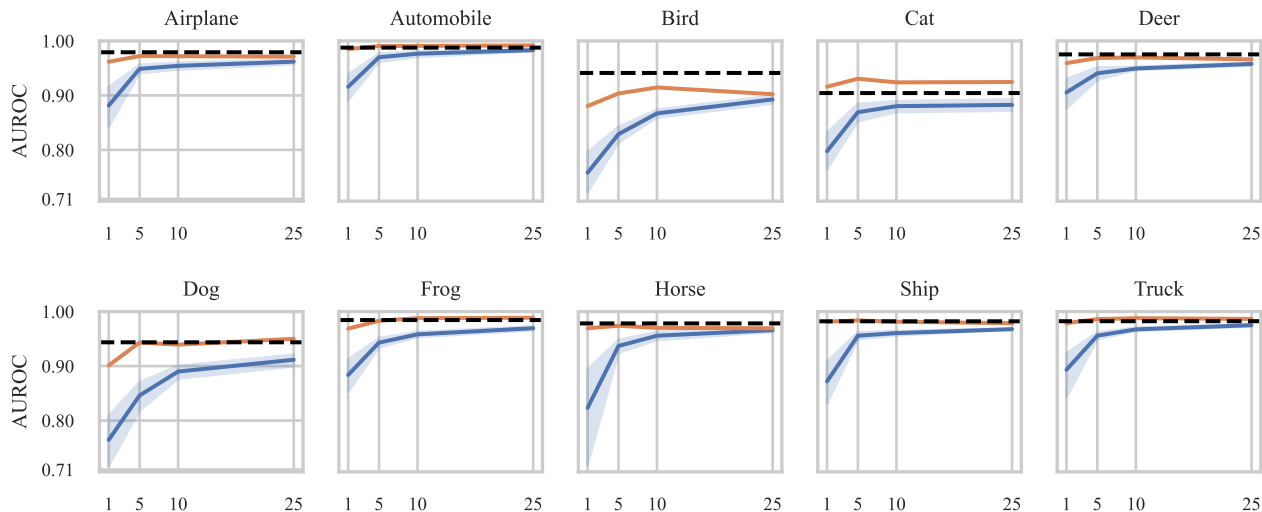


Figure 2. Only 10 representative training samples are needed to surpass the performance of training with the whole dataset on five out of the ten classes in CIFAR10. AUROC for training with 1, 5, 10, and 25 random (blue) or best (greedy selection; orange) samples on CIFAR10. For random samples, the experiments were repeated ten times with different samples. Dashed black line represents training with all 4000 ID samples.

|          | Dataset size | CIFAR10      | CIFAR100     | Fashion-MNIST | MNIST        | MVTec-AD      | BraTS         | RSNA / transfer               |
|----------|--------------|--------------|--------------|---------------|--------------|---------------|---------------|-------------------------------|
|          | 100%         | <b>96.58</b> | <b>94.92</b> | <b>95.79</b>  | <b>98.41</b> | <u>98.48</u>  | 98.75         | 81.81                         |
| Greedy   | 1            | 95.02        | 89.94        | 94.00         | 90.15        | 89.70         | 95.25         | 75.98 / 69.82                 |
|          | 5            | 96.36        | 92.49        | 95.31         | 93.62        | 91.52         | 97.25         | 78.61 / 77.52                 |
|          | 10           | <u>96.37</u> | 92.59        | 95.38         | 94.91        | 92.94         | 97.06         | 79.94 / 80.11                 |
|          | 25           | 96.29        | 92.60        | <u>95.52</u>  | 96.06        | 93.53         | 97.94         | 80.08 / 80.24                 |
| Evo      | 1            | 87.68        | 79.99        | 86.82         | 74.82        | 85.55         | 94.00         | 75.44 / 73.54                 |
|          | 5            | 94.30        | 90.40        | 93.42         | 92.96        | 94.12         | <b>99.06*</b> | 79.43 / 78.25                 |
|          | 10           | 95.51        | 91.78        | 94.28         | 95.37        | 96.37         | 98.81*        | <u>81.95*</u> / 80.62         |
|          | 25           | 95.51        | 91.88        | 95.07         | 97.30        | <b>98.52*</b> | <u>98.87*</u> | <b>83.09*</b> / <b>82.88*</b> |
| Core-set | 1            | 90.08        | 79.62        | 91.47         | 82.29        | -             | -             | -                             |
|          | 5            | 93.85        | 89.74        | 93.89         | 92.55        | -             | -             | -                             |
|          | 10           | 94.28        | 91.03        | 94.47         | 94.94        | -             | -             | -                             |
|          | 25           | 94.85        | <u>92.88</u> | 95.13         | <u>97.33</u> | -             | -             | -                             |
| Random   | 1            | 84.96 ±1.2   | 77.05 ±1.4   | 83.51 ±3.3    | 76.11 ±2.2   | 83.61 ±1.2    | 93.85 ±5.3    | 63.61 ±9.0                    |
|          | 5            | 91.95 ±0.7   | 86.40 ±0.8   | 91.86 ±1.1    | 89.36 ±1.1   | 90.43 ±0.9    | 97.83 ±1.1    | 77.18 ±2.4                    |
|          | 10           | 93.59 ±0.4   | 89.05 ±0.5   | 93.24 ±0.3    | 93.00 ±0.6   | 92.80 ±0.6    | 97.96 ±1.0    | 78.83 ±2.5                    |
|          | 25           | 94.68 ±0.2   | 91.52 ±0.2   | 94.16 ±0.2    | 96.24 ±0.3   | 95.29 ±0.3    | 98.09 ±0.6    | 80.59 ±0.9                    |

Table 1. AUROC scores of training with the full dataset and training with 1, 5, 10, and 25 best-performing (with greedy search, the evolutionary algorithm, and core-set selection) or random samples. Since the performance of randomly selected subgroups can vary strongly, we repeated these experiments over ten different subsets. Bold numbers show the best performance per dataset, and underlined numbers are the second-best. Numbers marked with \* surpass training with 100% of the data. The *transfer* column shows the best-performing RSNA samples found using RD but trained with FAE. Note that this table shows the averaged results over each class in the respective datasets. Detailed results for all classes can be found in the Appendix.

#### 4.4. The evolutionary algorithm covers a wider distribution of normal variations

Greedy selection is a fast and intuitive algorithm that gives great results on CIFAR10, CIFAR100, and Fashion-MNIST (c.f. Tab. 1). However, on MNIST, MVTec-AD, BraTS, and RSNA, it is outperformed by the evolutionary algorithm. In this section, we analyze the reasons for that: The evolutionary algorithm seems to be more suitable when the number of possible normal variations is low. The objects within each class of the MVTec-AD dataset are very similar and often only oriented differently, and the ChestX-ray images all show the same anatomical region. The brain MRI in BraTS are registered to an atlas and, consequently, have even lower anatomical variance. This is in contrast to CIFAR10, CIFAR100, and Fashion-MNIST, where the in-distribution training class can exhibit various shapes, poses, and colors. An impressive example of a failure case of the greedy selection is the *screw* category in MVTec-AD (c.f. Tab. 6 in the Appendix). Fig. 3 shows that greedy selection favors combinations of similarly oriented images, while the evolutionary algorithm better covers the different orientations that should all be considered normal. This helps the UAD model in discriminating different orientations of normal images from defects like deformations, scratches, or threads. However, as mentioned above, this seems to work best if the number of possible normal variations is low. The results on CIFAR10, CIFAR100, and Fashion-MNIST show that the evolutionary algorithm is noisy and at risk of also covering samples that degrade performance.

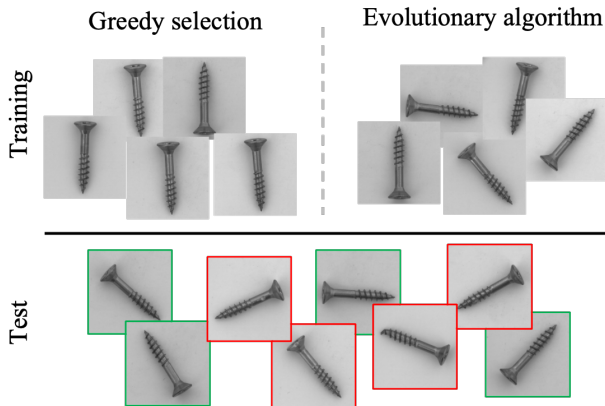


Figure 3. Greedy selection favors visually similar samples, while the evolutionary algorithm achieves a better coverage of the normal variations in the training dataset. Best five training samples for the screw-category in MVTec-AD found using greedy selection (left) and the evolutionary algorithm (right). Bottom: normal (green) and defective (red) samples in the test set.

#### 4.5. What characterizes normal samples?

Our methods not only allow training strong UAD models using only a few samples, it also provides insights into what constitutes a prototypical in-distribution image. Fig. 4 shows the best- and worst-performing samples for each class in CIFAR10. The “worst” images display well-light prototypical objects that are well centered, have good contrast, and mostly uniform backgrounds. In contrast, the “worst” ID images include drawings (bird and horse), toys (frog, truck), historical objects (plane, car), or images with bad contrast (dog).



Figure 4. Best- and worst-performing samples for each class in CIFAR10. Identified using greedy selection.

In noisy, less well-curated datasets like RSNA, our method can effectively detect and filter low-quality samples. Fig. 5 reveals severe deformations, external devices, low tissue contrast, or dislocations in the worst-performing samples. The best-performing ones, on the other side, are well-centered, detailed, contain male and female samples, and clearly show the lungs, a prerequisite for detecting pneumonia.



Figure 5. Best- and worst-performing samples in RSNA. Identified using the evolutionary algorithm.

#### 4.6. Manually creating a training dataset of prototypical samples

Motivated by the insights we gained about the characteristics of in-distribution samples, we manually selected a training subset with the aim of gaining high performance. We selected samples that had similar characteristics as displayed in Fig. 5 and covered the distribution of ID samples well. We chose the RSNA dataset for this experiment because it contains outliers compared to MVTec-AD and because the images were large enough to be visually inspected, in con-

trast to the other natural image datasets. We only started the evaluation of the manually selected samples once their selection was complete. No information other than the characteristics described in Sec. 4.5 was used for the manual selection, and the author selecting the samples was not a trained radiologist or other medical expert. When training with these manually selected samples, we achieved AUROCs of 55.75, 80.26, 81.95, and 82.31 for 1, 5, 10, and 25 samples, respectively, outperforming our greedy selection strategy, random selection, and training with 100% of the data.

We repeated a similar experiment for the – arbitrarily selected – “8” class on MNIST. This time, however, we did not look at the best- or worst-performing samples from this class, but simply selected samples that are visually close to a prototypical 8. We discarded samples that had non-closed lines, where the “bellies” of the 8 were too slim, and those with wiggly lines. As above, we only started the evaluation of these manually selected samples once their selection was complete. With these samples, we achieved AUROCs of 76.69, 92.42, 94.59, and 96.37 for 1, 5, 10, and 25 samples, respectively, outperforming both random selection and the evolutionary strategy, while also only falling 1.45 below full training performance.

#### 4.7. Surfaced samples are transferrable to other models and datasets

As described in Sec. 4.1, we also trained a Reverse Distillation (RD) model on RSNA. The last column in Tab. 1 shows how the best-performing samples surfaced with greedy selection and the evolutionary algorithm on RD perform when applied to the FAE model. Although RD overall performs worse than FAE (c.f. Tab. 2), its best-performing samples work well on FAE, performing almost on par with the ones found with FAE itself. We conclude from this result that there are commonalities between the best samples that are independent of the model. This means that samples found on one model can be transferred to another.

Similarly, high performance for sample combinations on RSNA translates well to the CheXpert dataset. As expected, training with RSNA samples gives a slightly lower performance on CheXpert than training on the CheXpert itself (red and black dashed lines in Fig. 6). This gap, however, can be closed by training with only 25 selected samples from RSNA. Even more impressive, we reached higher performance on CheXpert when training with the 25 manually selected RSNA samples than when training on the full CheXpert dataset itself.

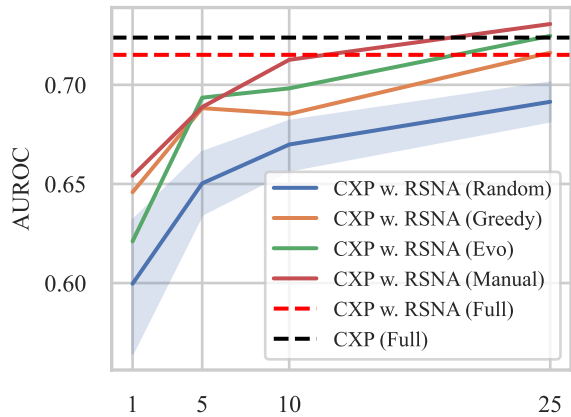


Figure 6. Training with 25 carefully selected samples from RSNA can exceed full training performance with CheXpert (8443 samples) when evaluated on the latter. Test performance on CheXpert after training on CheXpert samples (black, dashed line) or RSNA (other lines). “CXP w. RSNA” means training the UAD model with samples from RSNA and evaluating on CheXpert.

## 5. Discussion

### 5.1. Long-tail in-distribution samples can degrade anomaly detection performance

We hypothesize that the reason for this is due to the nature of the in-distributions, which often have long tails, as shown by Feldman [15], Zhu et al. [44]. Fig. 7 reveals that this might also be the case for the datasets used in our study. This means that the majority of the in-distribution samples have only low inter-sample variance, with the exception of a few rare samples that differ a lot from each other but are still part of the in-distribution. While these samples can be actively contrasted to other classes and memorized by supervised machine learning models [16], such mechanisms are not available for UAD models, where the long-tail in-distribution samples are treated as any other training sample. This can shift the decision boundary in an unfortunate way (cf. Fig. 8 b). Training with carefully selected samples effectively ignores these data points and leads to better performance despite using fewer samples (Fig. 8 c). Our hypothesis is complemented by the experiments in Fig. 4, where the worst-performing in-distribution samples for “airplane” and “automobile” are historical objects, thus likely laying at the tail of the in-distribution. The same theory can partly explain the good performance of the core-set selection strategy: The centroids of a fitted GMM are unlikely to be localized towards the tails of the distribution as only a few samples reside there.

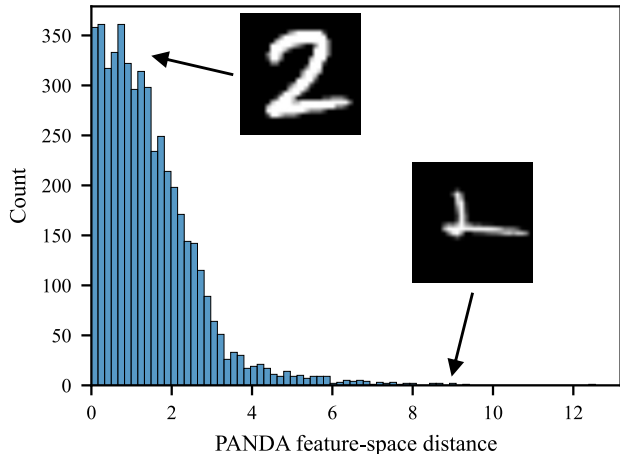


Figure 7. MNIST follows a long-tail distribution in the PANDA feature-space. Histogram of distances of all training samples from MNIST class “2” to the center of a PANDA model and two example images from the center and the tail.

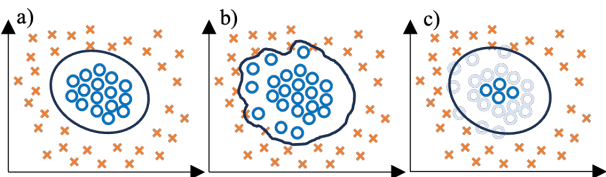


Figure 8. Training with only a few selected samples helps to ignore training samples that lie at the tails of the in-distribution. Illustration of our hypothesis of how long-tail in-distribution samples can skew the decision boundary. a) Ideal scenario: The in-distribution data is distinct from the OOD data. b) Some ID samples might be closer to the OOD data and shift the decision boundary. c) Training with a few carefully selected samples is closer to the ideal scenario.

## 5.2. Should samples from the long tails of the in-distribution be considered outliers?

Our experiments suggest that there are samples in the training datasets that lie at the tails of the in-distribution and lower the performance of the UAD model. Our subset-selection strategies are effective at filtering out these data points. Of course, ignoring such long-tail samples during training will declare them as outliers, which, at first sight, is false given the labels. Maybe, however, these data points should be considered as such because they should be treated with special care downstream. A downstream supervised classification algorithm, for example, is more likely to misclassify such samples. In that case, flagging long tail samples as OOD is desired. X-ray images as shown on the right of Fig. 5 can pose difficulties (even for manual diagnosis) and should also receive special attention. Further, as we have shown, including these samples during training can

lower the classification performance for other samples that are then falsely flagged as ID. The selection methods presented in this study can, therefore, not only be used to surface the most prototypical in-distribution samples but can also be used to automatically filter a dataset from noisy or corrupted images.

## 5.3. Why is training with small datasets attractive?

When only very few data samples are needed to successfully train a UAD model, this has profound effects on their usefulness. Small datasets can relatively easily be created with little effort. This lowers the entry bar for designing performant algorithms, especially for actors with few resources, thus contributing to the democratization of AI. It also makes more tasks potentially solvable where data is potentially very difficult or expensive to acquire.

## 6. Conclusion

In many domains of Deep Learning, the prevailing assumption is that more training data leads to better models. Our work challenges this practice for UAD and highlights the importance of data quality over data quantity. While the initial surfacing of prototypical samples proposed in this paper (with greedy selection and the evolutionary algorithm) was computationally expensive and required a labeled validation set, a key contribution of this work is the discovery that samples from the long tail of the training distribution can degrade performance and that only a fraction of the currently used training data is necessary for high performance. The characteristics of prototypical in-distribution samples that we derived further allow for manual selection and are transferrable across models, datasets, and even modalities and tasks. This understanding of the well-performing training samples can help in designing better UAD models in the future and in developing novel approaches that can perform the selection automatically and without the use of labels. Lastly, with the core-set selection strategy, we additionally presented such an approach (although so far just for one model), and if a slight drop in performance can be accepted, even randomly selecting a subset of training samples presents a viable solution.

## References

- [1] Davide Abati, Angelo Porrello, Simone Calderara, and Rita Cucchiara. Latent space autoregression for novelty detection. In *CVPR*, pages 481–490, 2019. 2
- [2] Samet Akcay, Amir Atapour-Abarghouei, and Toby P Breckon. Ganomaly: Semi-supervised anomaly detection via adversarial training. In *ACCV*, pages 622–637. Springer, 2019. 2
- [3] Jaehyeok Bae, Jae-Han Lee, and Seyun Kim. Pni: Industrial anomaly detection using position and neighborhood information. In *CVPR*, pages 6373–6383, 2023. 1, 2



- [4] Spyridon Bakas, Hamed Akbari, Aristeidis Sotiras, Michel Bilello, Martin Rozycki, Justin S Kirby, John B Freymann, Keyvan Farahani, and Christos Davatzikos. Advancing the cancer genome atlas glioma mri collections with expert segmentation labels and radiomic features. *Scientific data*, 4(1): 1–13, 2017. 4
- [5] Christoph Baur, Stefan Denner, Benedikt Wiestler, Nassir Navab, and Shadi Albarqouni. Autoencoders for unsupervised anomaly segmentation in brain mr images: a comparative study. *Medical Image Analysis*, 69:101952, 2021. 2
- [6] Cosmin I Bercea, Benedikt Wiestler, Daniel Rueckert, and Shadi Albarqouni. Federated disentangled representation learning for unsupervised brain anomaly detection. *Nature Machine Intelligence*, 4(8):685–695, 2022. 1
- [7] Liron Bergman and Yedid Hoshen. Classification-based anomaly detection for general data. *arXiv preprint arXiv:2005.02359*, 2020. 2
- [8] Liron Bergman, Niv Cohen, and Yedid Hoshen. Deep nearest neighbor anomaly detection. *arXiv preprint arXiv:2002.10445*, 2020. 2
- [9] Paul Bergmann, Sindy Löwe, Michael Fauser, David Sattlegger, and Carsten Steger. Improving unsupervised defect segmentation by applying structural similarity to autoencoders. *arXiv preprint arXiv:1807.02011*, 2018. 2
- [10] Paul Bergmann, Michael Fauser, David Sattlegger, and Carsten Steger. Mvtec ad — a comprehensive real-world dataset for unsupervised anomaly detection. In *CVPR*, pages 9584–9592, 2019. 1, 2, 4
- [11] Paul Bergmann, Michael Fauser, David Sattlegger, and Carsten Steger. Uninformed students: Student-teacher anomaly detection with discriminative latent embeddings. In *CVPR*, pages 4183–4192, 2020. 2
- [12] Lucas Deecke, Robert Vandermeulen, Lukas Ruff, Stephan Mandt, and Marius Kloft. Image anomaly detection with generative adversarial networks. In *Machine Learning and Knowledge Discovery in Databases: European Conference, ECML PKDD 2018, Dublin, Ireland, September 10–14, 2018, Proceedings, Part I 18*, pages 3–17. Springer, 2019. 2
- [13] Thomas Defard, Aleksandr Setkov, Angélique Loesch, and Romaric Audigier. Padim: a patch distribution modeling framework for anomaly detection and localization. In *International Conference on Pattern Recognition*, pages 475–489. Springer, 2021. 2
- [14] Hanqiu Deng and Xingyu Li. Anomaly detection via reverse distillation from one-class embedding. In *CVPR*, pages 9737–9746, 2022. 1, 2, 4
- [15] Vitaly Feldman. Does learning require memorization? a short tale about a long tail. In *Proceedings of the 52nd Annual ACM SIGACT Symposium on Theory of Computing*, pages 954–959, 2020. 7
- [16] Vitaly Feldman and Chiyuan Zhang. What neural networks memorize and why: Discovering the long tail via influence estimation. *NeurIPS*, 33:2881–2891, 2020. 7
- [17] Izhak Golan and Ran El-Yaniv. Deep anomaly detection using geometric transformations. *Advances in neural information processing systems*, 31, 2018. 2
- [18] Dong Gong, Lingqiao Liu, Vuong Le, Budhaditya Saha, Moussa Reda Mansour, Svetha Venkatesh, and Anton van den Hengel. Memorizing normality to detect anomaly: Memory-augmented deep autoencoder for unsupervised anomaly detection. In *CVPR*, pages 1705–1714, 2019. 2
- [19] Kaiming He, Xiangyu Zhang, Shaoqing Ren, and Jian Sun. Deep residual learning for image recognition. In *CVPR*, pages 770–778, 2016. 2, 1
- [20] Jeremy Irvin, Pranav Rajpurkar, Michael Ko, Yifan Yu, Silvana Ciurea-Ilcus, Chris Chute, Henrik Marklund, Behzad Haghgoo, Robyn Ball, Katie Shpanskaya, et al. Chexpert: A large chest radiograph dataset with uncertainty labels and expert comparison. In *Proceedings of the AAAI conference on artificial intelligence*, pages 590–597, 2019. 4
- [21] Ki Hyun Kim, Sangwoo Shim, Yongsub Lim, Jongseob Jeon, Jeongwoo Choi, Byungchan Kim, and Andre S Yoon. Rapp: Novelty detection with reconstruction along projection pathway. In *ICLR*, 2019. 2
- [22] Alex Krizhevsky, Geoffrey Hinton, et al. Learning multiple layers of features from tiny images. 2009. 2, 4
- [23] Ioannis Lagogiannis, Felix Meissen, Georgios Kaissis, and Daniel Rueckert. Unsupervised pathology detection: A deep dive into the state of the art. *IEEE Transactions on Medical Imaging*, pages 1–1, 2023. 1, 2, 4
- [24] Yann LeCun, Léon Bottou, Yoshua Bengio, and Patrick Haffner. Gradient-based learning applied to document recognition. *Proceedings of the IEEE*, 86(11):2278–2324, 1998. 2, 4
- [25] Chun-Liang Li, Kihyuk Sohn, Jinsung Yoon, and Tomas Pfister. Cutpaste: Self-supervised learning for anomaly detection and localization. In *CVPR*, pages 9664–9674, 2021. 2
- [26] Wenqian Liu, Runze Li, Meng Zheng, Srikrishna Karanam, Ziyang Wu, Bir Bhanu, Richard J Radke, and Octavia Camps. Towards visually explaining variational autoencoders. In *CVPR*, pages 8642–8651, 2020. 2
- [27] Yifan Mao, Fei-Fei Xue, Ruixuan Wang, Jianguo Zhang, Wei-Shi Zheng, and Hongmei Liu. Abnormality detection in chest x-ray images using uncertainty prediction autoencoders. In *MICCAI*, pages 529–538. Springer, 2020. 2
- [28] Felix Meissen, Johannes Paetzold, Georgios Kaissis, and Daniel Rueckert. Unsupervised anomaly localization with structural feature-autoencoders. In *Brainlesion: Glioma, Multiple Sclerosis, Stroke and Traumatic Brain Injuries*, pages 14–24, Cham, 2023. Springer Nature Switzerland. 1, 2, 4
- [29] Bjoern H Menze, Andras Jakab, Stefan Bauer, Jayashree Kalpathy-Cramer, Keyvan Farahani, Justin Kirby, Yuliya Burren, Nicole Porz, Johannes Slotboom, Roland Wiest, et al. The multimodal brain tumor image segmentation benchmark (brats). *IEEE transactions on medical imaging*, 34(10):1993–2024, 2014. 4
- [30] Baharan Mirzasoleiman, Jeff Bilmes, and Jure Leskovec. Coresets for data-efficient training of machine learning models. In *International Conference on Machine Learning*, pages 6950–6960. PMLR, 2020. 2

- [31] Pramuditha Perera, Ramesh Nallapati, and Bing Xiang. Ogan: One-class novelty detection using gans with constrained latent representations. In *CVPR*, pages 2898–2906, 2019. 2
- [32] Tal Reiss, Niv Cohen, Liron Bergman, and Yedid Hoshen. Panda: Adapting pretrained features for anomaly detection and segmentation. In *CVPR*, pages 2806–2814, 2021. 2, 4, 1
- [33] Karsten Roth, Latha Pemula, Joaquin Zepeda, Bernhard Schölkopf, Thomas Brox, and Peter Gehler. Towards total recall in industrial anomaly detection. In *CVPR*, pages 14318–14328, 2022. 1, 2, 4
- [34] Lukas Ruff, Robert Vandermeulen, Nico Goernitz, Lucas Deecke, Shoaib Ahmed Siddiqui, Alexander Binder, Emmanuel Müller, and Marius Kloft. Deep one-class classification. In *International conference on machine learning*, pages 4393–4402. PMLR, 2018. 2, 1
- [35] Thomas Schlegl, Philipp Seeböck, Sebastian M Waldstein, Georg Langs, and Ursula Schmidt-Erfurth. f-anogan: Fast unsupervised anomaly detection with generative adversarial networks. *Medical image analysis*, 54:30–44, 2019. 1, 2
- [36] Anouk Stein, Carol Wu, Chris Carr, George Shih, Jamie Dulkowski, Jayashree Kalpathy-Cramer, Leon Chen, Luciano Prevedello, Marc Kohli, Mark McDonald, et al. Rsna pneumonia detection challenge, 2018. 4, 1
- [37] Max Welling. Herding dynamical weights to learn. In *Proceedings of the 26th Annual International Conference on Machine Learning*, pages 1121–1128, 2009. 2
- [38] Julian Wyatt, Adam Leach, Sebastian M Schmon, and Chris G Willcocks. Anoddpn: Anomaly detection with denoising diffusion probabilistic models using simplex noise. In *CVPR*, pages 650–656, 2022. 2
- [39] Han Xiao, Kashif Rasul, and Roland Vollgraf. Fashion-mnist: a novel image dataset for benchmarking machine learning algorithms, 2017. 2, 4
- [40] Suhang You, Kerem C Tezcan, Xiaoran Chen, and Ender Konukoglu. Unsupervised lesion detection via image restoration with a normative prior. In *International Conference on Medical Imaging with Deep Learning*, pages 540–556. PMLR, 2019. 2
- [41] Vitjan Zavrtanik, Matej Kristan, and Danijel Skočaj. Draema: a discriminatively trained reconstruction embedding for surface anomaly detection. In *CVPR*, pages 8330–8339, 2021. 2
- [42] Jianpeng Zhang, Yutong Xie, Yi Li, Chunhua Shen, and Yong Xia. Covid-19 screening on chest x-ray images using deep learning based anomaly detection. *arXiv preprint arXiv:2003.12338*, 27(10.48550), 2020. 2
- [43] Chong Zhou and Randy C Paffenroth. Anomaly detection with robust deep autoencoders. In *Proceedings of the 23rd ACM SIGKDD international conference on knowledge discovery and data mining*, pages 665–674, 2017. 2
- [44] Xiangxin Zhu, Dragomir Anguelov, and Deva Ramanan. Capturing long-tail distributions of object subcategories. In *CVPR*, pages 915–922, 2014. 7
- [45] David Zimmerer, Fabian Isensee, Jens Petersen, Simon Kohl, and Klaus Maier-Hein. Unsupervised anomaly localization using variational auto-encoders. In *Medical Image Computing and Computer Assisted Intervention–MICCAI 2019:*

*22nd International Conference, Shenzhen, China, October 13–17, 2019, Proceedings, Part IV 22*, pages 289–297. Springer, 2019. 2

# How Low Can You Go? Surfacing Prototypical In-Distribution Samples for Unsupervised Anomaly Detection

## Supplementary Material

### 7. Datasets

#### CIFAR10, CIFAR100, MNIST, and FashionMNIST

We follow the widely used training setup from Reiss et al. [32] for these datasets. CIFAR10 contains 6000 images per class. For each class  $c \in C$ , we create a training dataset  $D_c$  using 4000 samples from said class. The remaining samples are split equally into a validation and a test set and combined with the same amount of samples from every other class as outliers. Training, validation, and test sets for CIFAR100, MNIST, and Fashion-MNIST are created analogous. For CIFAR100, we used the 20 superclasses instead of the 100 detailed classes.

**MVTec-AD** MVTEC-AD is a dataset for defect detection in industrial production. Here, we used the original splits as outlined by Bergmann et al. [10].

**BraTS** The multimodal brain tumor image segmentation benchmark (BraTS) contains 369 MRI from patients with glioma. We extract 5 slices around the center-line and use only 101 slices without glioma for training. The remaining 80 normal slices are split 50:50 into a validation and a test set and are complemented with 40 pathological slices each. Following Meissen et al. [28], we use the T2-weighted sequences, perform histogram equalization on the slices and resize them to  $128 \times 128$ .

**RSNA and CheXpert** The RSNA Pneumonia Detection dataset [36] is a subset of 30 000 frontal view chest radiographs from the National Institutes of Health (NIH) CXR8 dataset that was manually labelled by 18 radiologists for one of the following labels: “Normal”, “Lung Opacity”, or “No Lung Opacity / Not Normal”. The CheXpert database contains 224 316 chest radiographs of 65 240 patients acquired at Stanford Hospital with 13 structured diagnostic labels. To make the CheXpert compatible with RSNA, we only considered frontal-view images without support devices and further excluded those where any of the labels is marked as uncertain. In addition to the image data and labels, demographic information about the patients’ gender and age were available for both datasets. We followed Lagogiannis et al. [23] *et al.* in categorizing patients into groups of young (< 32 years) and old (> 60 years).

For RSNA, we used the “Normal” label as in-distribution images and combined the “pneumonia” and “No Opacity/Not Normal” (has lung opacities, but not suspicious

for pneumonia) as OOD. Similarly, for CheXpert, the “No Finding” label was used as in-distribution, and “pneumonia” and “lung opacity” as OOD. For both datasets, we created a validation- and a test-set that are balanced w.r.t. gender (male and female), age (young and old), the presence of anomalies, and contain 800 samples each. The remaining in-distribution samples were used for training. As part of preprocessing, all Chest X-ray images were center cropped and resized to  $128 \times 128$  pixels. Note that we treated both datasets individually and did not combine them for training or evaluation.

### 8. Models

**PANDA** PANDA [32] is a model built upon DeepSVDD by Ruff et al. [34]. Like the latter, it relies on training a one-class classifier by using the compactness loss. Given a feature-extractor  $\psi$  and a center vector  $c$ , the compactness loss is defined as:

$$\mathcal{L}_{\text{compact}} = \sum_{x \in D} \|\psi(x) - c\|^2. \quad (6)$$

The center vector  $c$  is computed as the mean feature vector of the training dataset  $D$  on the untrained model  $\psi_0$ :

$$c = \frac{1}{|D|} \sum_{x \in D} \psi_0(x). \quad (7)$$

Instead of training a specialized architecture from scratch, PANDA benefits from useful features of pre-trained models. Specifically, it extracts features from the penultimate layer of a ResNet152 [19] and categorizes samples into normal / anomal by the L1-distance to the  $k$  nearest neighbors (kNN), with  $k = 2$ . PANDA only fine-tunes layer3 and layer4 and uses early stopping to determine the optimal distance between ID and OOD samples. Training has no effect when using only one sample as the feature representation of the only sample is always identical to  $c$ . We used the original configuration from their paper for our experiments.

**PatchCore** PatchCore [33] follows a similar concept as PANDA. However, instead of performing kNN search on pooled, global features, PatchCore achieves localized anomaly detection by using a memory bank of locally-aware patch features  $\mathcal{M}$ , instead. To make the kNN search

computationally feasible, PatchCore performs core-set selection on the memory bank to retain only a subset of representative features  $\mathcal{M}_{\text{sub}}$ :

$$\mathcal{M}_{\text{sub}}^* = \arg \min_{\mathcal{M}_{\text{sub}} \subset \mathcal{M}} \max_{m \in \mathcal{M}} \min_{n \in \mathcal{M}_{\text{sub}}} \|m - n\|_2. \quad (8)$$

Compared to PANDA, PatchCore does not require fine-tuning of the feature extractor. We used the same hyperparameters for PatchCore as in the original publication.

**FAE** The Structural Feature-Autoencoder (FAE) [28] extracts spatial feature maps from a pre-trained and frozen feature extractor  $\psi$  (a ResNet18 [19] in practice). The feature-maps are resized and concatenated and fed into a convolutional autoencoder  $f_\theta$  that is trained via the structural similarity (SSIM) loss for reconstruction:

$$\mathcal{L} = \text{SSIM}(\psi(x), f_\theta(\psi(x))). \quad (9)$$

Anomalies are detected using the residual between the feature-maps and their reconstruction like in popular image-reconstruction models. It was found to perform best for UAD in Chest X-ray images in a study by Lagogiannis et al. [23]. We use a smaller model in our experiments, since it still gave us the same performance on the RSNA full dataset as the larger model and is more resource-efficient. Specifically, we set the `fae_hidden_dims` parameter to [50, 100]. The other parameters were kept the same as in the original publication.

**Reverse Distillation** The Reverse Distillation (RD) model by Deng and Li [14] utilizes a frozen encoder model and a decoder that mirrors the former, similar to an Autoencoder. Instead of reconstructing the image, however, RD minimizes the cosine distance between feature-maps in the encoder and decoder. The same measure is also used during inference to detect anomalies. RD was the second-best performing UAD model for Chest X-ray images in Lagogiannis et al. [23]. We used the same hyperparameters for RD as in Lagogiannis et al. [23].

## 9. Transferring samples between models

### 10. Detailed results

We show the results for RD on RSNA in Tab. 2 and the detailed per-class results for CIFAR10, CIFAR100, MNIST, Fashion-MNIST, and MVTEC-AD in Tabs. 3 to 6, respectively.

|        | Dataset size | RSNA / transfer             |
|--------|--------------|-----------------------------|
|        | 100%         | 71.96                       |
| Greedy | 1            | 63.34 / 58.20               |
|        | 5            | 71.86 / 67.10               |
|        | 10           | 71.89 / 68.25               |
|        | 25           | <b>73.39</b> / 72.83        |
| Evo    | 1            | 65.28 / 70.58               |
|        | 5            | 70.03 / 71.89               |
|        | 10           | 71.17 / <u>74.14</u>        |
|        | 25           | <u>72.93</u> / <b>74.36</b> |
| Random | 1            | 52.51 ±6.9                  |
|        | 5            | 65.31 ±4.5                  |
|        | 10           | 67.22 ±3.9                  |
|        | 25           | 70.07 ±2.0                  |

Table 2. Results for RD on RSNA. AUROC scores of full training and training with 1, 5, 10, 25 best-performing (with greedy search and evolutionary algorithm) or random samples. Since the performance of randomly selected subgroups can vary strongly, we repeated these experiments over ten different subsets. Best performances are marked in bold, second-best underlined. The *transfer* column shows best-performing samples found using FAE, but trained with RD.

|          | Dataset size | Airplane        | Automobile      | Bird            | Cat             | Deer            | Dog             | Frog            | Horse            | Ship            | Truck           | Average         |
|----------|--------------|-----------------|-----------------|-----------------|-----------------|-----------------|-----------------|-----------------|------------------|-----------------|-----------------|-----------------|
|          | 100%         | <b>97.92</b>    | 98.76           | <b>94.12</b>    | 90.43           | <b>97.53</b>    | <u>94.36</u>    | 98.44           | <b>97.83</b>     | <u>98.21</u>    | 98.23           | <b>96.58</b>    |
| Greedy   | 1            | 96.18           | 98.50           | 88.04           | 91.59           | 95.92           | 90.13           | 96.87           | 96.94            | 98.14           | 97.88           | 95.02           |
|          | 5            | <u>97.22</u>    | 99.05           | <b>90.36</b>    | <b>93.06</b>    | 96.86           | 94.32           | 98.31           | 97.39            | <b>98.37</b>    | 98.61           | 96.36           |
|          | 10           | 97.19           | <u>99.08</u>    | <u>91.45</u>    | <u>92.39</u>    | <u>96.97</u>    | 93.94           | <u>98.79</u>    | 97.01            | 98.14           | <b>98.79</b>    | <u>96.37</u>    |
|          | 25           | 97.11           | <b>99.17</b>    | <u>90.22</u>    | 92.46           | 96.61           | <b>95.00</b>    | <b>98.87</b>    | 96.93            | 97.87           | <u>98.65</u>    | <u>96.29</u>    |
| Evo      | 1            | 86.15           | 97.08           | 88.04           | 78.61           | 93.27           | 79.83           | 67.29           | 94.21            | 96.64           | 95.73           | 87.68           |
|          | 5            | 95.85           | 96.60           | 89.19           | 87.44           | 96.12           | 92.23           | 93.89           | 97.11            | 96.72           | 97.88           | 94.30           |
|          | 10           | 96.47           | 97.98           | 90.64           | 89.32           | 96.62           | 93.61           | 97.72           | 96.93            | 97.62           | 98.23           | 95.51           |
|          | 25           | 96.56           | 98.18           | 91.38           | 89.16           | 96.68           | 92.11           | 97.87           | <u>97.42</u>     | 97.64           | 98.08           | 95.51           |
| Core-set | 1            | 94.54           | 96.86           | 79.14           | 81.56           | 92.75           | 84.63           | 92.84           | 92.28            | 92.09           | 94.15           | 90.08           |
|          | 5            | 94.14           | 97.23           | 88.70           | 87.88           | 95.91           | 90.36           | 95.24           | 96.39            | 96.22           | 96.46           | 93.85           |
|          | 10           | 94.90           | 97.79           | 88.56           | 88.09           | 95.91           | 91.50           | 96.31           | 96.46            | 96.45           | 96.81           | 94.28           |
|          | 25           | 96.88           | 98.67           | 89.06           | 86.26           | 95.98           | 92.98           | 97.40           | 96.99            | 96.68           | 97.56           | 94.85           |
| Random   | 1            | 88.14 $\pm 6.3$ | 91.59 $\pm 4.1$ | 75.81 $\pm 6.2$ | 79.75 $\pm 5.5$ | 90.55 $\pm 4.7$ | 76.47 $\pm 7.6$ | 88.38 $\pm 5.1$ | 82.34 $\pm 15.1$ | 87.19 $\pm 6.6$ | 89.32 $\pm 7.6$ | 84.96 $\pm 1.2$ |
|          | 5            | 94.88 $\pm 1.3$ | 97.00 $\pm 1.2$ | 82.88 $\pm 2.4$ | 86.92 $\pm 2.7$ | 94.06 $\pm 2.0$ | 84.61 $\pm 4.5$ | 94.30 $\pm 1.5$ | 93.68 $\pm 2.0$  | 95.57 $\pm 1.1$ | 95.58 $\pm 1.0$ | 91.95 $\pm 0.7$ |
|          | 10           | 95.42 $\pm 1.2$ | 97.65 $\pm 0.8$ | 86.70 $\pm 1.2$ | 88.02 $\pm 1.6$ | 94.94 $\pm 0.5$ | 89.00 $\pm 2.0$ | 95.82 $\pm 0.8$ | 95.57 $\pm 1.3$  | 96.05 $\pm 0.7$ | 96.74 $\pm 0.5$ | 93.59 $\pm 0.4$ |
|          | 25           | 96.19 $\pm 0.7$ | 98.30 $\pm 0.3$ | 89.26 $\pm 1.2$ | 88.26 $\pm 1.7$ | 95.77 $\pm 0.5$ | 91.16 $\pm 1.9$ | 96.95 $\pm 0.6$ | 96.59 $\pm 0.5$  | 96.77 $\pm 0.2$ | 97.50 $\pm 0.3$ | 94.68 $\pm 0.2$ |

Table 3. Detailed training results for CIFAR10. AUROC scores of full training and training with 1, 5, 10, 25 best-performing (with greedy search, the evolutionary algorithm, and core-set selection) or random samples. Since the performance of randomly selected subgroups can vary strongly, we repeated these experiments over ten different subsets. Best performances are marked in bold, second-best underlined.

|          | Dataset size | 0               | 1               | 2                | 3               | 4                | 5               | 6               | 7               | 8               | 9               | Average         |
|----------|--------------|-----------------|-----------------|------------------|-----------------|------------------|-----------------|-----------------|-----------------|-----------------|-----------------|-----------------|
|          | 100%         | <b>99.84</b>    | <b>99.93</b>    | <b>96.58</b>     | <b>98.02</b>    | <u>98.63</u>     | <b>96.45</b>    | <u>99.13</u>    | <b>99.14</b>    | <u>97.82</u>    | <b>98.53</b>    | <b>98.41</b>    |
| Greedy   | 1            | 98.14           | 97.09           | 82.74            | 89.92           | 92.94            | 88.69           | 85.01           | 87.87           | 89.59           | 89.53           | 90.15           |
|          | 5            | 99.21           | 98.29           | 85.59            | 93.13           | 95.65            | 90.90           | 93.00           | 92.52           | 94.31           | 93.56           | 93.62           |
|          | 10           | 99.43           | 98.83           | 89.00            | 93.99           | 96.89            | 91.39           | 95.62           | 93.97           | 96.28           | 93.75           | 94.91           |
|          | 25           | 99.67           | 99.30           | 89.85            | 96.63           | 97.67            | 90.84           | 98.32           | 94.88           | <b>97.86</b>    | 95.60           | 96.06           |
| Evo      | 1            | 82.31           | 83.30           | 69.87            | 75.18           | 78.13            | 82.36           | 78.57           | 59.38           | 62.56           | 76.56           | 74.82           |
|          | 5            | 98.76           | 96.96           | 85.06            | 94.82           | 95.78            | 91.44           | 95.57           | 89.28           | 87.35           | 94.59           | 92.96           |
|          | 10           | 99.40           | 99.30           | 88.08            | 94.42           | 97.97            | 92.40           | 97.59           | 97.28           | 92.17           | 95.09           | 95.37           |
|          | 25           | 99.44           | <u>99.72</u>    | 91.65            | <u>97.09</u>    | <b>99.01</b>     | 95.10           | <b>99.23</b>    | <u>98.70</u>    | 95.43           | <u>97.60</u>    | 97.30           |
| Core-set | 1            | 94.71           | 92.27           | 71.53            | 86.66           | 80.33            | 78.28           | 75.39           | 76.65           | 82.48           | 84.61           | 82.29           |
|          | 5            | 99.29           | 99.58           | 86.83            | 92.32           | 89.07            | 91.30           | 94.72           | 91.68           | 91.88           | 88.82           | 92.55           |
|          | 10           | 99.38           | 99.66           | 90.60            | 94.23           | 96.27            | 91.46           | 95.65           | 93.56           | 93.45           | 95.16           | 94.94           |
|          | 25           | <u>99.76</u>    | 99.71           | <u>92.42</u>     | 96.22           | 97.04            | <u>95.96</u>    | 98.89           | 98.66           | 97.37           | 97.23           | <u>97.33</u>    |
| Random   | 1            | 91.11 $\pm 2.4$ | 90.34 $\pm 6.0$ | 65.18 $\pm 10.6$ | 77.02 $\pm 4.4$ | 69.79 $\pm 11.2$ | 69.69 $\pm 9.7$ | 69.43 $\pm 6.9$ | 70.37 $\pm 7.6$ | 76.91 $\pm 3.6$ | 81.26 $\pm 5.4$ | 76.11 $\pm 2.2$ |
|          | 5            | 98.52 $\pm 0.9$ | 97.79 $\pm 2.2$ | 77.40 $\pm 7.3$  | 89.79 $\pm 1.9$ | 90.25 $\pm 1.9$  | 85.58 $\pm 4.9$ | 88.90 $\pm 4.3$ | 86.97 $\pm 2.6$ | 87.92 $\pm 3.5$ | 90.42 $\pm 2.1$ | 89.36 $\pm 1.1$ |
|          | 10           | 98.86 $\pm 0.6$ | 99.18 $\pm 0.4$ | 83.04 $\pm 4.0$  | 92.39 $\pm 2.0$ | 93.82 $\pm 2.3$  | 90.84 $\pm 1.3$ | 92.81 $\pm 2.8$ | 93.28 $\pm 1.2$ | 92.34 $\pm 1.8$ | 93.40 $\pm 1.1$ | 93.00 $\pm 0.6$ |
|          | 25           | 99.38 $\pm 0.2$ | 99.70 $\pm 0.1$ | 90.26 $\pm 2.1$  | 95.36 $\pm 1.5$ | 96.66 $\pm 1.0$  | 93.37 $\pm 1.0$ | 97.55 $\pm 1.3$ | 97.49 $\pm 0.5$ | 95.83 $\pm 0.6$ | 96.79 $\pm 0.5$ | 96.24 $\pm 0.3$ |

Table 4. Detailed training results for MNIST. AUROC scores of full training and training with 1, 5, 10, 25 best-performing (with greedy search, the evolutionary algorithm, and core-set selection) or random samples. Since the performance of randomly selected subgroups can vary strongly, we repeated these experiments over ten different subsets. Best performances are marked in bold, second-best underlined.

|          | Dataset size | 0                | 1               | 2                | 3               | 4                | 5               | 6                | 7               | 8               | 9               | Average         |
|----------|--------------|------------------|-----------------|------------------|-----------------|------------------|-----------------|------------------|-----------------|-----------------|-----------------|-----------------|
|          | 100%         | <b>95.09</b>     | <b>99.52</b>    | 94.44            | <b>96.28</b>    | <b>93.66</b>     | 96.58           | 85.33            | <b>99.28</b>    | <b>98.88</b>    | 98.86           | <b>95.79</b>    |
| Greedy   | 1            | 93.85            | 98.12           | 93.03            | 88.85           | 90.46            | 97.14           | 84.55            | 98.84           | 95.99           | 99.16           | 94.00           |
|          | 5            | 94.64            | 98.98           | 94.27            | 92.38           | 92.95            | 97.98           | 86.42            | 99.18           | 96.84           | 99.42           | 95.31           |
|          | 10           | 94.79            | 98.98           | 94.53            | 93.38           | 92.00            | <b>98.55</b>    | <u>86.74</u>     | <u>99.27</u>    | 96.02           | <u>99.50</u>    | 95.38           |
|          | 25           | <u>95.06</u>     | 99.03           | <b>94.64</b>     | 94.49           | <u>92.97</u>     | <u>98.54</u>    | <b>86.76</b>     | 99.26           | 94.86           | <b>99.60</b>    | <u>95.52</u>    |
| Evo      | 1            | 89.28            | 83.19           | 88.71            | 83.60           | 79.98            | 94.35           | 71.09            | 96.53           | 84.16           | 97.30           | 86.82           |
|          | 5            | 92.74            | 98.85           | 93.94            | 89.42           | 88.10            | 94.19           | 83.62            | 98.59           | 96.30           | 98.43           | 93.42           |
|          | 10           | 91.41            | <u>99.31</u>    | <u>94.57</u>     | 94.72           | 90.11            | 95.62           | 82.86            | 98.93           | 96.90           | 98.37           | 94.28           |
|          | 25           | 94.10            | 99.24           | 94.12            | <u>95.15</u>    | <u>92.97</u>     | 95.70           | 84.11            | 98.94           | 97.32           | 99.00           | 95.07           |
| Core-set | 1            | 90.94            | 97.12           | 91.63            | 83.53           | 88.62            | 95.75           | 76.01            | 98.67           | 94.42           | 98.00           | 91.47           |
|          | 5            | 92.05            | 97.95           | 92.91            | 91.24           | 89.85            | 97.32           | 84.05            | 98.61           | 96.10           | 98.87           | 93.89           |
|          | 10           | 93.77            | 98.85           | 94.14            | 92.82           | 91.40            | 96.13           | 84.14            | 98.72           | 95.98           | 98.70           | 94.47           |
|          | 25           | 94.40            | 99.18           | 94.16            | 94.70           | 91.64            | 97.07           | 84.80            | 99.13           | <u>97.37</u>    | 98.87           | 95.13           |
| Random   | 1            | 77.24 $\pm$ 11.0 | 96.45 $\pm$ 0.8 | 82.47 $\pm$ 17.5 | 73.80 $\pm$ 7.5 | 75.09 $\pm$ 12.5 | 91.63 $\pm$ 4.1 | 69.29 $\pm$ 12.4 | 94.71 $\pm$ 6.2 | 79.04 $\pm$ 8.4 | 95.37 $\pm$ 4.6 | 83.51 $\pm$ 3.3 |
|          | 5            | 90.58 $\pm$ 3.7  | 97.90 $\pm$ 0.5 | 92.13 $\pm$ 1.8  | 85.24 $\pm$ 5.4 | 88.77 $\pm$ 1.3  | 95.38 $\pm$ 1.9 | 80.89 $\pm$ 2.4  | 98.34 $\pm$ 0.8 | 91.01 $\pm$ 6.7 | 98.41 $\pm$ 1.2 | 91.86 $\pm$ 1.1 |
|          | 10           | 91.78 $\pm$ 2.1  | 98.31 $\pm$ 0.5 | 93.22 $\pm$ 0.9  | 89.62 $\pm$ 2.4 | 89.87 $\pm$ 0.7  | 96.24 $\pm$ 1.3 | 81.83 $\pm$ 1.9  | 98.57 $\pm$ 0.7 | 94.31 $\pm$ 1.6 | 98.62 $\pm$ 0.7 | 93.24 $\pm$ 0.3 |
|          | 25           | 93.28 $\pm$ 1.2  | 98.62 $\pm$ 0.3 | 93.74 $\pm$ 0.7  | 93.37 $\pm$ 1.6 | 91.48 $\pm$ 0.9  | 95.86 $\pm$ 1.0 | 82.45 $\pm$ 1.4  | 98.89 $\pm$ 0.2 | 95.31 $\pm$ 1.0 | 98.62 $\pm$ 0.5 | 94.16 $\pm$ 0.2 |

Table 5. Detailed training results for Fashion-MNIST. AUROC scores of full training and training with 1, 5, 10, 25 best-performing (with greedy search, the evolutionary algorithm, and core-set selection) or random samples. Since the performance of randomly selected subgroups can vary strongly, we repeated these experiments over ten different subsets. Best performances are marked in bold, second-best underlined.

|        | Dataset size | Bottle                  | Cable           | Capsule         | Carpet          | Grid            | Hazelnut        | Leather                 | Metal nut       |
|--------|--------------|-------------------------|-----------------|-----------------|-----------------|-----------------|-----------------|-------------------------|-----------------|
|        | 100%         | <b>100.00</b>           | <b>99.53</b>    | <b>99.20</b>    | 98.43           | <u>99.08</u>    | <b>100.00</b>   | <b>100.00</b>           | <b>99.90</b>    |
| Greedy | 1            | 99.76                   | 88.19           | 72.80           | 98.60           | 71.19           | 93.93           | <b>100.00</b>           | 72.19           |
|        | 5            | <b>100.00</b>           | 96.27           | 84.96           | <u>98.64</u>    | 73.52           | 98.29           | <b>100.00</b>           | 97.75           |
|        | 10           | <b>100.00</b>           | 97.58           | 93.06           | 98.15           | 78.86           | 99.64           | <b>100.00</b>           | 98.92           |
|        | 25           | <b>100.00</b>           | 96.74           | 93.94           | 98.27           | 83.88           | <u>99.71</u>    | <b>100.00</b>           | 99.41           |
| Evo    | 1            | 99.52                   | 88.92           | 63.14           | 98.23           | 66.88           | 93.04           | <b>100.00</b>           | 70.97           |
|        | 5            | 99.52                   | 93.22           | 90.91           | 98.19           | 86.04           | 99.14           | <b>100.00</b>           | 98.34           |
|        | 10           | <b>100.00</b>           | 96.42           | 91.26           | 98.39           | 94.40           | <b>100.00</b>   | <b>100.00</b>           | 99.07           |
|        | 25           | <b>100.00</b>           | <u>98.29</u>    | 94.34           | 98.56           | <b>99.11</b>    | <b>100.00</b>   | <b>100.00</b>           | <u>99.76</u>    |
| Random | 1            | 99.71 $\pm$ 0.1         | 83.74 $\pm$ 4.7 | 66.80 $\pm$ 5.1 | 97.72 $\pm$ 0.5 | 60.30 $\pm$ 6.9 | 90.67 $\pm$ 2.6 | <u>99.99</u> $\pm$ 0.0  | 71.99 $\pm$ 4.0 |
|        | 5            | 99.84 $\pm$ 0.2         | 91.40 $\pm$ 3.6 | 84.11 $\pm$ 7.2 | 97.98 $\pm$ 0.3 | 72.64 $\pm$ 7.1 | 96.29 $\pm$ 2.2 | <b>100.00</b> $\pm$ 0.0 | 94.93 $\pm$ 3.5 |
|        | 10           | <u>99.90</u> $\pm$ 0.2  | 93.49 $\pm$ 1.8 | 90.29 $\pm$ 2.3 | 98.04 $\pm$ 0.3 | 80.91 $\pm$ 5.7 | 98.99 $\pm$ 0.7 | <b>100.00</b> $\pm$ 0.0 | 97.72 $\pm$ 1.6 |
|        | 25           | <b>100.00</b> $\pm$ 0.0 | 96.59 $\pm$ 1.0 | 93.61 $\pm$ 1.5 | 98.14 $\pm$ 0.3 | 90.23 $\pm$ 2.9 | 99.81 $\pm$ 0.3 | <b>100.00</b> $\pm$ 0.0 | 99.20 $\pm$ 0.4 |
|        | Dataset size | Pill                    | Screw           | Tile            | Toothbrush      | Transistor      | Wood            | Zipper                  | Average         |
|        | 100%         | <b>96.21</b>            | <b>97.13</b>    | <u>99.96</u>    | 90.28           | <b>99.62</b>    | 98.77           | 99.11                   | <u>98.48</u>    |
| Greedy | 1            | 89.23                   | 55.87           | <b>100.00</b>   | 88.61           | 91.42           | 99.21           | 99.37                   | 89.70           |
|        | 5            | 89.77                   | 53.40           | <b>100.00</b>   | 87.22           | 94.46           | 99.30           | 99.16                   | 91.52           |
|        | 10           | 93.43                   | 53.68           | <b>100.00</b>   | 85.56           | 96.38           | 99.30           | <b>99.58</b>            | 92.94           |
|        | 25           | 94.03                   | 54.44           | <b>100.00</b>   | 85.56           | 98.17           | 99.21           | <u>99.55</u>            | 93.53           |
| Evo    | 1            | 72.64                   | 52.96           | 99.13           | 90.00           | 92.12           | 99.04           | 96.61                   | 85.55           |
|        | 5            | 91.41                   | 61.47           | 99.49           | 98.33           | 97.58           | 99.30           | 98.90                   | 94.12           |
|        | 10           | 93.40                   | 75.90           | 99.71           | <u>99.44</u>    | <u>99.58</u>    | <u>99.39</u>    | 98.58                   | 96.37           |
|        | 25           | <u>95.23</u>            | <u>95.43</u>    | 98.77           | <b>99.72</b>    | 99.50           | <b>99.56</b>    | <u>99.55</u>            | <b>98.52</b>    |
| Random | 1            | 78.71 $\pm$ 5.0         | 46.22 $\pm$ 4.8 | 99.59 $\pm$ 0.5 | 82.58 $\pm$ 3.5 | 83.31 $\pm$ 4.7 | 98.18 $\pm$ 0.7 | 94.58 $\pm$ 1.5         | 83.61 $\pm$ 1.2 |
|        | 5            | 89.48 $\pm$ 2.0         | 52.86 $\pm$ 5.1 | 99.87 $\pm$ 0.1 | 87.22 $\pm$ 5.2 | 93.77 $\pm$ 1.7 | 98.57 $\pm$ 0.4 | 97.55 $\pm$ 1.5         | 90.43 $\pm$ 0.9 |
|        | 10           | 90.95 $\pm$ 1.8         | 58.42 $\pm$ 4.0 | 99.89 $\pm$ 0.1 | 90.75 $\pm$ 1.1 | 95.86 $\pm$ 1.8 | 98.60 $\pm$ 0.2 | 98.13 $\pm$ 1.0         | 92.80 $\pm$ 0.6 |
|        | 25           | 93.73 $\pm$ 1.1         | 72.89 $\pm$ 4.0 | 99.94 $\pm$ 0.1 | 90.06 $\pm$ 0.6 | 97.88 $\pm$ 0.7 | 98.62 $\pm$ 0.2 | 98.64 $\pm$ 0.6         | 95.29 $\pm$ 0.3 |

Table 6. Detailed training results for MVTec-AD. AUROC scores of full training and training with 1, 5, 10, 25 best-performing (with greedy search and evolutionary algorithm) or random samples. Since the performance of randomly selected subgroups can vary strongly, we repeated these experiments over ten different subsets. Best performances are marked in bold, second-best underlined.

|          | Dataset size | Aquatic mammals              | Fish                           | Flowers              | Food containers          | Fruit and vegetables | Household electrical devices | Household furniture | Insects          | Large carnivores | Large man-made outdoor things |
|----------|--------------|------------------------------|--------------------------------|----------------------|--------------------------|----------------------|------------------------------|---------------------|------------------|------------------|-------------------------------|
| Greedy   | 100%         | <u>93.68</u>                 | <b>94.81</b>                   | 98.46                | <u>95.86</u>             | <b>96.59</b>         | <b>94.59</b>                 | <b>97.26</b>        | <b>93.00</b>     | <b>95.34</b>     | 94.98                         |
|          | 1            | 91.93                        | 89.09                          | 96.78                | 89.39                    | 90.97                | 85.73                        | 96.17               | 84.78            | 92.46            | 93.98                         |
|          | 5            | <b>94.13</b>                 | 92.32                          | 98.13                | 95.59                    | 93.00                | 85.05                        | 96.78               | 91.05            | <u>93.73</u>     | <u>95.55</u>                  |
|          | 10           | 93.84                        | 91.92                          | <b>98.60</b>         | <b>95.97</b>             | 92.88                | 82.56                        | 96.81               | 89.68            | <u>93.33</u>     | <b>95.57</b>                  |
|          | 25           | 92.36                        | 91.27                          | <u>98.50</u>         | 95.79                    | 92.53                | 80.51                        | <b>97.26</b>        | <u>90.89</u>     | 93.21            | 95.45                         |
| Evo      | 1            | 89.68                        | 78.96                          | 80.31                | 76.69                    | 84.76                | 80.61                        | 92.09               | 63.07            | 85.80            | 90.19                         |
|          | 5            | 93.04                        | 89.85                          | 97.08                | 85.89                    | 92.47                | 89.12                        | 95.64               | 86.96            | 90.11            | 93.78                         |
|          | 10           | 93.19                        | 89.98                          | 98.16                | 91.44                    | 93.24                | 88.27                        | <u>96.86</u>        | 88.92            | 90.95            | 93.79                         |
|          | 25           | 92.88                        | <u>92.50</u>                   | 98.39                | 92.87                    | <u>95.00</u>         | 90.37                        | 96.84               | 90.74            | 91.84            | 94.29                         |
| Core-set | 1            | 64.34                        | 75.71                          | 90.52                | 80.05                    | 85.14                | 73.08                        | 90.44               | 61.80            | 68.79            | 89.97                         |
|          | 5            | 86.53                        | 88.90                          | 96.48                | 91.79                    | 91.29                | 86.67                        | 95.75               | 87.01            | 91.77            | 92.95                         |
|          | 10           | 91.31                        | 90.85                          | 97.41                | 92.08                    | 92.28                | 86.71                        | 95.99               | 85.73            | 92.60            | 94.00                         |
|          | 25           | 91.72                        | 91.87                          | 98.23                | 94.68                    | 94.94                | <u>90.80</u>                 | 96.21               | 90.31            | 93.09            | 93.92                         |
| Random   | 1            | 71.70 $\pm$ 14.7             | 75.23 $\pm$ 8.1                | 90.83 $\pm$ 3.9      | 82.25 $\pm$ 3.7          | 71.29 $\pm$ 12.5     | 71.88 $\pm$ 7.1              | 84.70 $\pm$ 6.1     | 68.09 $\pm$ 12.3 | 77.95 $\pm$ 11.7 | 86.72 $\pm$ 6.0               |
|          | 5            | 86.25 $\pm$ 3.8              | 81.82 $\pm$ 6.1                | 95.82 $\pm$ 1.4      | 89.31 $\pm$ 2.4          | 85.26 $\pm$ 5.9      | 78.90 $\pm$ 6.2              | 92.54 $\pm$ 2.0     | 79.26 $\pm$ 9.0  | 87.47 $\pm$ 1.7  | 92.15 $\pm$ 1.5               |
|          | 10           | 88.50 $\pm$ 1.9              | 85.56 $\pm$ 4.8                | 96.97 $\pm$ 0.7      | 91.31 $\pm$ 1.7          | 90.59 $\pm$ 3.1      | 80.97 $\pm$ 4.3              | 94.77 $\pm$ 0.8     | 81.96 $\pm$ 5.0  | 90.22 $\pm$ 1.4  | 92.49 $\pm$ 1.2               |
|          | 25           | 90.04 $\pm$ 1.3              | 90.78 $\pm$ 1.2                | 97.87 $\pm$ 0.5      | 93.19 $\pm$ 1.5          | 93.63 $\pm$ 0.6      | 84.21 $\pm$ 4.1              | 96.28 $\pm$ 0.5     | 86.34 $\pm$ 1.7  | 91.82 $\pm$ 0.8  | 93.50 $\pm$ 0.6               |
|          | Dataset size | Large natural outdoor scenes | Large omnivores and herbivores | Medium-sized mammals | Non-insect invertebrates | People               | Reptiles                     | Small mammals       | Trees            | Vehicles 1       | Vehicles 2                    |
| Greedy   | 100%         | 95.37                        | <b>94.40</b>                   | <b>93.54</b>         | <b>90.76</b>             | <b>98.55</b>         | <b>91.71</b>                 | <b>92.70</b>        | 96.84            | <b>96.06</b>     | <b>93.88</b>                  |
|          | 1            | 94.13                        | 86.01                          | 84.57                | 79.51                    | 96.20                | 79.39                        | 88.86               | 95.92            | 93.20            | 89.81                         |
|          | 5            | 94.98                        | 90.29                          | 89.08                | 82.67                    | 97.90                | 84.47                        | <u>92.49</u>        | 96.89            | 95.61            | 90.10                         |
|          | 10           | 95.49                        | 89.41                          | 90.43                | 85.01                    | 98.18                | 87.55                        | 91.98               | <u>97.67</u>     | <u>95.92</u>     | 88.95                         |
|          | 25           | <b>95.84</b>                 | 90.23                          | 90.78                | <u>86.55</u>             | 98.13                | <u>89.72</u>                 | 91.81               | 97.50            | 95.87            | 87.78                         |
| Evo      | 1            | 88.88                        | 78.12                          | 73.68                | 77.34                    | 83.52                | 52.97                        | 86.70               | 95.58            | 68.73            | 72.15                         |
|          | 5            | 95.11                        | 87.96                          | 83.67                | 81.76                    | 97.33                | 81.79                        | 90.32               | 96.83            | 92.12            | 87.22                         |
|          | 10           | 94.95                        | 89.90                          | 88.72                | 83.32                    | 97.69                | 85.42                        | 90.41               | 97.48            | 94.83            | 88.14                         |
|          | 25           | 95.44                        | 91.58                          | <u>91.27</u>         | 85.68                    | 97.97                | 88.61                        | 91.33               | 97.17            | 95.64            | 90.17                         |
| Core-set | 1            | 93.57                        | 74.96                          | 79.55                | 56.37                    | 91.10                | 72.36                        | 87.23               | 94.28            | 82.56            | 80.49                         |
|          | 5            | 93.92                        | 86.92                          | 87.56                | 75.77                    | 95.14                | 85.19                        | 86.94               | 95.48            | 92.46            | 86.36                         |
|          | 10           | <u>95.81</u>                 | 86.39                          | 87.80                | 79.06                    | 96.93                | 86.52                        | 89.47               | 96.81            | 93.88            | 89.05                         |
|          | 25           | <u>95.81</u>                 | <u>91.72</u>                   | 90.12                | 83.86                    | 97.56                | 88.04                        | 90.91               | <b>97.84</b>     | 94.60            | <u>91.28</u>                  |
| Random   | 1            | 86.87 $\pm$ 6.3              | 66.79 $\pm$ 14.8               | 73.91 $\pm$ 7.6      | 60.08 $\pm$ 8.3          | 88.73 $\pm$ 6.4      | 66.99 $\pm$ 7.5              | 72.46 $\pm$ 9.3     | 92.30 $\pm$ 3.6  | 78.59 $\pm$ 8.2  | 73.74 $\pm$ 6.6               |
|          | 5            | 92.30 $\pm$ 2.0              | 82.54 $\pm$ 3.3                | 84.66 $\pm$ 2.1      | 71.37 $\pm$ 5.1          | 95.66 $\pm$ 1.2      | 79.22 $\pm$ 3.2              | 85.18 $\pm$ 4.6     | 95.67 $\pm$ 0.9  | 88.96 $\pm$ 3.2  | 83.75 $\pm$ 3.8               |
|          | 10           | 93.76 $\pm$ 1.2              | 85.27 $\pm$ 2.7                | 87.79 $\pm$ 1.3      | 78.13 $\pm$ 2.9          | 96.39 $\pm$ 0.8      | 83.14 $\pm$ 3.0              | 87.63 $\pm$ 2.7     | 96.44 $\pm$ 0.5  | 92.30 $\pm$ 1.8  | 86.80 $\pm$ 1.5               |
|          | 25           | 94.93 $\pm$ 0.7              | 89.69 $\pm$ 1.5                | 89.68 $\pm$ 0.6      | 83.07 $\pm$ 1.6          | 97.47 $\pm$ 0.5      | 86.95 $\pm$ 1.1              | 89.92 $\pm$ 0.8     | 97.06 $\pm$ 0.3  | 94.09 $\pm$ 0.4  | 89.90 $\pm$ 1.0               |

Table 7. Detailed training results for CIFAR100. AUROC scores of full training and training with 1, 5, 10, 25 best-performing (with greedy search, the evolutionary algorithm, and core-set selection) or random samples. Since the performance of randomly selected subgroups can vary strongly, we repeated these experiments over ten different subsets. Best performances are marked in bold, second-best underlined.